



**HAL**  
open science

## **Pervasive aqueous alteration in the early Solar System revealed by potassium isotopic variations in Ryugu samples and carbonaceous chondrites**

Yan Hu, Frédéric Moynier, Wei Dai, Marine Paquet, Tetsuya Yokoyama, Yoshinari Abe, Jérôme Aléon, Conel M. O'D. Alexander, Sachiko Amari, Yuri Amelin, et al.

### ► To cite this version:

Yan Hu, Frédéric Moynier, Wei Dai, Marine Paquet, Tetsuya Yokoyama, et al.. Pervasive aqueous alteration in the early Solar System revealed by potassium isotopic variations in Ryugu samples and carbonaceous chondrites. *Icarus*, 2023, 409, pp.115884. <10.1016/j.icarus.2023.115884>. <hal-04616201>

**HAL Id: hal-04616201**

**<https://hal.science/hal-04616201v1>**

Submitted on 18 Jun 2024

**HAL** is a multi-disciplinary open access archive for the deposit and dissemination of scientific research documents, whether they are published or not. The documents may come from teaching and research institutions in France or abroad, or from public or private research centers.

L'archive ouverte pluridisciplinaire **HAL**, est destinée au dépôt et à la diffusion de documents scientifiques de niveau recherche, publiés ou non, émanant des établissements d'enseignement et de recherche français ou étrangers, des laboratoires publics ou privés.



HAL Authorization

1 **Pervasive aqueous alteration in the early Solar System revealed by**  
2 **potassium isotopic variations in Ryugu samples and carbonaceous chondrites**

3  
4 Yan Hu<sup>1,\*</sup>, Frédéric Moynier<sup>1,\*</sup>, Wei Dai<sup>1</sup>, Marine Paquet<sup>1</sup>, Tetsuya Yokoyama<sup>2</sup>, Yoshinari  
5 Abe<sup>3</sup>, Jérôme Aléon<sup>4</sup>, Conel M. O'D. Alexander<sup>5</sup>, Sachiko Amari<sup>6,7</sup>, Yuri Amelin<sup>8</sup>, Ken-ichi  
6 Bajo<sup>9</sup>, Martin Bizzarro<sup>10,1</sup>, Audrey Bouvier<sup>11</sup>, Richard W. Carlson<sup>12</sup>, Marc Chaussidon<sup>1</sup>, Byeon-  
7 Gak Choi<sup>12</sup>, Nicolas Dauphas<sup>13</sup>, Andrew M. Davis<sup>13</sup>, Tommaso Di Rocco<sup>14</sup>, Wataru Fujiya<sup>15</sup>,  
8 Ryota Fukai<sup>16</sup>, Ikshu Gautam<sup>2</sup>, Makiko K. Haba<sup>2</sup>, Yuki Hibiya<sup>17</sup>, Hiroshi Hidaka<sup>18</sup>, Hisashi  
9 Homma<sup>19</sup>, Peter Hoppe<sup>20</sup>, Gary R. Huss<sup>21</sup>, Kiyohiro Ichida<sup>22</sup>, Tsuyoshi Iizuka<sup>23</sup>, Trevor R.  
10 Ireland<sup>24</sup>, Akira Ishikawa<sup>2</sup>, M. Ito<sup>24</sup>, Shoichi Itoh<sup>25</sup>, Noriyuki Kawasaki<sup>9</sup>, Noriko T. Kita<sup>26</sup>, Kouki  
11 Kitajima<sup>26</sup>, Thorsten Kleine<sup>27</sup>, Shintaro Komatani<sup>22</sup>, Alexander N. Krot<sup>21</sup>, Ming-Chang Liu<sup>28</sup>,  
12 Yuki Masuda<sup>2</sup>, Kevin D. McKeegan<sup>28</sup>, Mayu Morita<sup>22</sup>, Kazuko Motomura<sup>29</sup>, Izumi Nakai<sup>30</sup>,  
13 Kazuhide Nagashima<sup>21</sup>, David Nesvorný<sup>30</sup>, Ann Nguyen<sup>31</sup>, Larry Nittler<sup>5</sup>, Morihiko Onose<sup>22</sup>,  
14 Andreas Pack<sup>14</sup>, Changkun Park<sup>32</sup>, Laurette Piani<sup>33</sup>, Liping Qin<sup>34</sup>, Sara S. Russell<sup>35</sup>, Naoya  
15 Sakamoto<sup>36</sup>, Maria Schönbächler<sup>37</sup>, Lauren Tafla<sup>29</sup>, Haolan Tang<sup>29</sup>, Kentaro Terada<sup>38</sup>, Yasuko  
16 Terada<sup>39</sup>, Tomohiro Usui<sup>16</sup>, Sohei Wada<sup>9</sup>, Meenakshi Wadhwa<sup>40</sup>, Richard J. Walker<sup>41</sup>, Katsuyuki  
17 Yamashita<sup>42</sup>, Qing-Zhu Yin<sup>43</sup>, Shigekazu Yoneda<sup>44</sup>, Edward D. Young<sup>29</sup>, Hiroharu Yui<sup>45</sup>, Ai-  
18 Cheng Zhang<sup>46</sup>, Tomoki Nakamura<sup>47</sup>, Hiroshi Naraoka<sup>48</sup>, Takaaki Noguchi<sup>25</sup>, Ryuji Okazaki<sup>48</sup>,  
19 Kanako Sakamoto<sup>16</sup>, Hikaru Yabuta<sup>49</sup>, Masanao Abe<sup>16</sup>, Akiko Miyazaki<sup>16</sup>, Aiko Nakato<sup>16</sup>,  
20 Masahiro Nishimura<sup>16</sup>, Tatsuaki Okada<sup>16</sup>, Toru Yada<sup>16</sup>, Kasumi Yogata<sup>16</sup>, Satoru Nakazawa<sup>16</sup>,  
21 Takanao Saiki<sup>16</sup>, Satoshi Tanaka<sup>16</sup>, Fuyuto Terui<sup>51</sup>, Yuichi Tsuda<sup>16</sup>, Sei-ichiro Watanabe<sup>18</sup>,  
22 Makoto Yoshikawa<sup>16</sup>, Shogo Tachibana<sup>51</sup>, Hisayoshi Yurimoto<sup>9</sup>

23 **Affiliations**

24 <sup>1</sup>Université Paris Cité, Institut de Physique du Globe de Paris, CNRS, 75005 Paris, France

25 <sup>2</sup>Department of Earth and Planetary Sciences, Tokyo Institute of Technology, Tokyo 152-8551, Japan.

26 <sup>3</sup>Graduate School of Engineering Materials Science and Engineering, Tokyo Denki University, Tokyo 120-  
27 8551, Japan.

28 <sup>4</sup>Institut de Minéralogie, de Physique des Matériaux et de Cosmochimie, Sorbonne Université, Museum  
29 National d'Histoire Naturelle, CNRS UMR 7590, IRD, 75005 Paris, France.

30 <sup>5</sup>Earth and Planets Laboratory, Carnegie Institution for Science, Washington, DC, 20015, USA.

31 <sup>6</sup>McDonnell Center for the Space Sciences and Physics Department, Washington University, St. Louis, MO  
32 63130, USA.

33 <sup>7</sup>Geochemical Research Center, The University of Tokyo, Tokyo, 113-0033, Japan.

34 <sup>8</sup>Guangzhou Institute of Geochemistry, Chinese Academy of Sciences, Guangzhou, GD 510640, China.

35 <sup>9</sup>Natural History Sciences, IIL, Hokkaido University, Sapporo 001-0021, Japan.

36 <sup>10</sup>Centre for Star and Planet Formation, GLOBE Institute, University of Copenhagen, Copenhagen, K 1350,  
37 Denmark.

38 <sup>11</sup>Bayerisches Geoinstitut, Universität Bayreuth, Bayreuth 95447, Germany.

39 <sup>12</sup>Department of Earth Science Education, Seoul National University, Seoul 08826, Republic of Korea.

40 <sup>13</sup>Department of the Geophysical Sciences and Enrico Fermi Institute, The University of Chicago, 5734  
41 South Ellis Avenue, Chicago 60637, USA.

42 <sup>14</sup>Faculty of Geosciences and Geography, University of Göttingen, Göttingen, D-37077, Germany.

43 <sup>15</sup>Faculty of Science, Ibaraki University, Mito 310-8512, Japan.

44 <sup>16</sup>ISAS/JSEC, JAXA, Sagami-hara 252-5210, Japan.

45 <sup>17</sup>General Systems Studies, The University of Tokyo, Tokyo 153-0041, Japan.

46 <sup>18</sup>Earth and Planetary Sciences, Nagoya University, Nagoya 464-8601, Japan.

47 <sup>19</sup>Osaka Application Laboratory, SBUWDX, Rigaku Corporation, Osaka 569-1146, Japan.

48 <sup>20</sup>Max Planck Institute for Chemistry, Mainz 55128, Germany.

49 <sup>21</sup>Hawai'i Institute of Geophysics and Planetology, University of Hawai'i at Mānoa; Honolulu, HI 96822,  
50 USA.

51 <sup>22</sup>Analytical Technology, Horiba Techno Service Co., Ltd., Kyoto 601-8125, Japan.

52 <sup>23</sup>Earth and Planetary Science, The University of Tokyo, Tokyo 113-0033, Japan.

53 <sup>24</sup>School of Earth and Environmental Sciences, The University of Queensland, St Lucia QLD 4072,  
54 Australia.

55 <sup>25</sup>Kochi Institute for Core Sample Research, JAMSTEC, Kochi 783-8502, Japan

56 <sup>26</sup>Earth and Planetary Sciences, Kyoto University, Kyoto 606-8502, Japan.

57 <sup>27</sup>Geoscience, University of Wisconsin-Madison, Madison, WI 53706, USA.

58 <sup>28</sup>Max Planck Institute for Solar System Research, 37077 Göttingen, Germany.

59 <sup>29</sup>Earth, Planetary, and Space Sciences, UCLA, Los Angeles, CA 90095, USA.

60 <sup>30</sup>Thermal Analysis, Rigaku Corporation, Tokyo 196-8666, Japan.

61 <sup>31</sup>Department of Space Studies, Southwest Research Institute, Boulder, CO 80302, USA.

62 <sup>32</sup>Astromaterials Research and Exploration Science, NASA Johnson Space Center; Houston, TX 77058,  
63 USA.

64 <sup>33</sup>Earth-System Sciences, Korea Polar Research Institute, Incheon 21990, Korea.

65 <sup>34</sup>Centre de Recherches Pétrographiques et Géochimiques, CNRS - Université de Lorraine, 54500 Nancy,  
66 France.

67 <sup>35</sup>University of Science and Technology of China, School of Earth and Space Sciences, Anhui 230026,  
68 China.

69 <sup>36</sup>Department of Earth Sciences, Natural History Museum, London, SW7 5BD, UK.

70 <sup>37</sup>IIL, Hokkaido University, Sapporo 001-0021, Japan.

71 <sup>38</sup>Institute for Geochemistry and Petrology, Department of Earth Sciences, ETH Zurich, Zurich,  
72 Switzerland.

73 <sup>39</sup>Earth and Space Science, Osaka University, Osaka 560-0043, Japan.

74 <sup>40</sup>Spectroscopy and Imaging, Japan Synchrotron Radiation Research Institute, Hyogo 679-5198 Japan.

75 <sup>41</sup>School of Earth and Space Exploration, Arizona State University, Tempe, AZ 85281, USA.

- 76 <sup>42</sup>Geology, University of Maryland, College Park, MD 20742, USA.
- 77 <sup>43</sup>Graduate School of Natural Science and Technology, Okayama University, Okayama 700-8530, Japan.
- 78 <sup>44</sup>Earth and Planetary Sciences, University of California, Davis, CA 95616, USA.
- 79 <sup>45</sup>Science and Engineering, National Museum of Nature and Science, Tsukuba 305-0005, Japan.
- 80 <sup>46</sup>Chemistry, Tokyo University of Science, Tokyo 162-8601, Japan.
- 81 <sup>47</sup>School of Earth Sciences and Engineering, Nanjing University, Nanjing 210023, China.
- 82 <sup>48</sup>Department of Earth Science, Tohoku University, Sendai, 980-8578, Japan.
- 83 <sup>49</sup>Department of Earth and Planetary Sciences, Kyushu University, Fukuoka 819-0395, Japan.
- 84 <sup>50</sup>Earth and Planetary Systems Science Program, Hiroshima University, Higashi-Hiroshima, 739-8526,
- 85 Japan.
- 86 <sup>51</sup>Kanagawa Institute of Technology, Atsugi 243-0292, Japan.
- 87 <sup>52</sup>UTokyo Organization for Planetary and Space Science, University of Tokyo, Tokyo 113-0033, Japan.

88  
89

Abstract: 183 words

Main text: 4070 words

Figures: 3

Table: 1

Submit to *Icarus*

(August, 2023)

96 \_\_\_\_\_

97 \*Corresponding authors:

98 Email: yanhu@ipgp.fr; moynier@ipgp.fr

99 **Abstract**

100 C-type asteroids are the presumed home to carbonaceous chondrites, some of which contain  
101 abundant life-forging volatiles and organics. For the first time, samples from a C-type asteroid  
102 (162173 Ryugu) were successfully returned to Earth by JAXA's Hayabusa2 mission. These  
103 pristine samples, uncontaminated by the terrestrial environment, allow a direct comparison with  
104 carbonaceous chondrites. This study reports the K isotopic compositions (expressed as  $\delta^{41}\text{K}$ ) of  
105 Ryugu samples and seven carbonaceous chondrites to constrain the origin of K isotopic variations  
106 in the early Solar System. Three aliquots of Ryugu particles collected at two touchdown sites have  
107 identical  $\delta^{41}\text{K}$  values, averaged at  $-0.194 \pm 0.038\%$  (2SD). The K isotopic composition of Ryugu  
108 falls within the range of  $\delta^{41}\text{K}$  values measured on representative CI chondrites, and together, they  
109 define an average  $\delta^{41}\text{K}$  value of  $-0.178 \pm 0.075\%$  (95% c.i.), which provides the current best  
110 estimate of the K isotopic composition of the bulk Solar System. Samples of CI chondrites with  
111  $\delta^{41}\text{K}$  values that deviate from this range likely reflect terrestrial contaminations or compositional  
112 heterogeneities at sampled sizes. In addition to CI chondrites, substantial K isotopic variability is  
113 observed in other carbonaceous chondrites and within individual chondritic groups, with  $\delta^{41}\text{K}$   
114 values inversely correlated with K abundances in many cases. These observations indicate  
115 widespread fluid activity in chondrite parent bodies, which significantly altered the original K  
116 abundances and isotopic compositions of chondrules and matrices established at their accretion.

117

118 **Keywords:** Asteroid Ryugu; Hayabusa2 mission; Carbonaceous chondrites; Stable potassium  
119 isotopes; Aqueous alteration

## 120 **1 Introduction**

121 Primitive asteroids accreted varying amounts of ice that melted to water-rich fluids due to heat  
122 released from the radioactive decay of short-lived nuclides (e.g.,  $^{26}\text{Al}$ , McSween et al., 2002) and  
123 possibly from impacts (Rubin, 2012). Consequently, fluid activity is believed to have been  
124 pervasive in the early history of planetesimal and planet development (Brearley, 2006; Brearley,  
125 2014; Clayton, 1993; Zolensky and McSween, 1988). Potassium (K) is a fluid-mobile, large-ion  
126 lithophile element that resides primarily in the metastasis and fine-grained matrix in carbonaceous  
127 asteroids. These components react readily with aqueous fluids, leading to redistribution of  $\text{K}^+$  and  
128 its isotopes. In addition, K is a moderately volatile metal that is variably depleted in carbonaceous  
129 chondrites and terrestrial planets. Because both volatility-driven depletion and fluid-rock  
130 interaction can lead to mass-dependent fractionations between the two stable K isotopes (i.e.,  $^{39}\text{K}$   
131 and  $^{41}\text{K}$ ), it is essential to understand how these processes affect  $\delta^{41}\text{K}$  variations in meteorites to  
132 facilitate the interpretation of K isotopic signatures of planetary materials.

133 Carbonaceous Ivuna-type (CI) chondrites are the chemically most primitive meteorites and  
134 have been widely used for inferring the isotopic composition of the bulk Solar System (Palme et  
135 al., 2014). Despite their primitive bulk composition, CI chondrites underwent near-complete  
136 aqueous alteration of anhydrous precursors to secondary mineral assemblages dominated by  
137 phyllosilicates (e.g., Tomeoka and Buseck, 1988) and display significant small-scale chemical  
138 heterogeneities (e.g., Barrat et al., 2012; Morlok et al., 2006; Palme and Zipfel, 2022). Because CI  
139 chondrites are limited in numbers and masses, and are susceptible to terrestrial modification,  
140 previous K isotopic analyses on them yielded inconsistent results. Earlier analyses of Orgueil, the  
141 largest CI witnessed fall (14 kg), returned a  $\delta^{41}\text{K}$  value ( $-0.534 \pm 0.097\%$ , 2SE) that is similar to  
142 the bulk Silicate Earth (Wang and Jacobsen, 2016). Later studies found that this terrestrial-like  
143  $\delta^{41}\text{K}$  value of Orgueil reflects K contamination on Earth, and other Orgueil samples have  $\delta^{41}\text{K}$   
144 values varying between  $-0.290\%$  and  $-0.039\%$  (Hu et al., 2022; Hu et al., 2023; Koefoed et al.,  
145 2023; Koefoed et al., 2022; Ku and Jacobsen, 2020; Nie et al., 2021). Two separate analyses on  
146 Ivuna also yielded markedly different  $\delta^{41}\text{K}$  values of  $-0.460 \pm 0.046\%$  (Nie et al., 2021) and  
147  $-0.180 \pm 0.060\%$  (Koefoed et al., 2023). The cause of this intra-group difference remains unclear.  
148 It may reflect an unrepresentative sampling of the bulk composition due to sample heterogeneity  
149 caused by aqueous alteration in the parent body(s) of the CI chondrites or remobilization of K in

150 terrestrial environments. A better-defined K isotopic composition of CI chondrites is critical for  
151 constraining the bulk composition of the Solar System.

152 In December 2020, JAXA's Hayabusa2 mission returned the first samples from the  
153 carbonaceous asteroid 162173 Ryugu, which had not been exposed to terrestrial environments  
154 prior to laboratory analysis. These samples contain abundant organic material plausibly inherited  
155 from the protosolar nebula and/or the interstellar medium, which attests to their primitive nature  
156 (Nakamura et al., 2022; Pilorget et al., 2022). Furthermore, chemical and isotopic analyses suggest  
157 that Ryugu has a similar bulk composition to CI chondrites (Hopp et al., 2022; Moynier et al.,  
158 2022; Nakamura et al., 2022; Paquet et al., 2022; Yokoyama et al., 2022). In particular, the Ryugu  
159 samples do not contain chondrules or refractory inclusions (Pilorget et al., 2022; Yokoyama et al.,  
160 2022) and display no depletion of volatile metals relative to the solar photosphere (Yokoyama et  
161 al., 2022), which are essential features of CI chondrites. Therefore, the Ryugu samples are a direct  
162 asteroidal analogue to CI chondrites, providing unique insights into the pristine composition of CI  
163 chondrites and the origin of K isotopic variability in the Solar System.

164 Here, we report the K isotopic compositions of three aliquots of Ryugu particles collected from  
165 two touchdown sites and seven carbonaceous chondrites measured with the Nu Sapphire collision-  
166 cell multi-collector inductively coupled plasma mass spectrometer (CC-MC-ICP-MS). We found  
167 that the Ryugu samples and CI chondrites have similar  $\delta^{41}\text{K}$  values, except for a significantly lower  
168 value previously reported for Ivuna. This finding further strengthens the isotopic links between  
169 Ryugu and CI chondrites. The large discrepancy in the  $\delta^{41}\text{K}$  values reported for Ivuna may reflect  
170 an unrepresentative bulk composition acquired on this sample. Fluid-rock interactions were likely  
171 widespread and heterogeneous in the parent bodies of the carbonaceous chondrites, which also  
172 resulted in considerable K isotopic variability in the CM (Mighei-type), CO (Ornans-type), CV  
173 (Vigarano-type), and CK (Karoonda-type) chondrites.

174

## 175 **2 Samples and methods**

### 176 **2.1 Sample description and pre-chemistry preparation**

177 Ryugu formed as a rubble-pile asteroid (approximately 1 km in diameter) reaccumulated from  
178 the shattered debris of a larger parent body (Sugita et al., 2019); therefore, Ryugu likely sampled  
179 rock fragments from all depths of its parent body. The Hayabusa2 mission retrieved 5.4 g of

180 pebbles and sands at two locations on Ryugu (Tachibana et al., 2022; Yada et al., 2022). Around  
181 3 g of surface material was collected from the touchdown site 1 and stored in Chamber A (Morota  
182 et al., 2020). The second landing targeted at collecting impact ejecta from a ~ 15-m diameter crater  
183 artificially made by the onboard Small Carry-on Impactor (SCI) (Arakawa et al., 2020). Around 2  
184 g of samples containing subsurface material was collected from the touchdown site 2 and stored  
185 in Chamber C. Samples collected from these two sites are considered representative of the  
186 compositionally homogeneous Ryugu surface based on their consistent spectral features and  
187 physical properties (color, shape, surface morphology, and structure) with onboard measurements  
188 made by the spacecraft (Kitazato et al., 2019; Nakamura et al., 2022; Pilonget et al., 2022;  
189 Tachibana et al., 2022).

190 Three aliquots of Ryugu particles were analyzed for K isotopes. Sample A0106 is from  
191 Chamber A, while samples C0107 and C0108 are from Chamber C. Preliminary sample treatment  
192 has been performed at the Tokyo Institute of Technology (Tokyo Tech). Samples A0106 and  
193 C0107 were first treated to extract soluble organic matter (Naraoka et al., 2023). Then, together  
194 with C0108, they were dissolved in precleaned perfluoroalkoxy (PFA) vials in a mixture of  
195 concentrated HF and HNO<sub>3</sub>, as described in Yokoyama et al. (2022). All three Ryugu samples  
196 were first processed to separate the Zn fractions from other constituent elements in the samples  
197 (Paquet et al., 2022). This was followed by a three-step sequential chemical separation procedure  
198 for the isotopic measurements of Fe (Hopp et al., 2022), Ti, and Cr (Yokoyama et al., 2022), after  
199 which we obtained a fraction containing K, Mg, and Ni. Aliquots of the K-Mg-Ni fraction for the  
200 Ryugu samples were transferred to the Institut de Physique du Globe de Paris (IPGP) for K isotopic  
201 analyses. The amounts of K finally obtained from the three Ryugu samples ranged from 1365 to  
202 2867 ng. To verify whether the multi-stage chemical separation fractionated the K isotopes, the K-  
203 Mg-Ni fractions of three carbonaceous chondrites, including Tarda (C2-ungrouped), Tagish Lake  
204 (C2-ungrouped), and Allende (CV3), which were subjected to the same processing as the Ryugu  
205 samples at Tokyo Tech, were chemically purified for K isotopic analyses at IPGP.

206 We also analyzed four geostandards (BIR, BCR-2, AGV-2, and seawater) and seven in-house  
207 carbonaceous chondrites at IPGP to examine possible sample heterogeneity and to compare with  
208 the K isotopic compositions of the Ryugu samples. The additional chondrite samples were: Orgueil  
209 (CI1), Tagish Lake (C2-ungrouped), Tarda (C2-ungrouped), Cold Bokkeveld (CM2), Murchison  
210 (CM2), Lance (CO3.5), and Allende (CV3). At IPGP, approximately 8-15 mg of the sample

211 powders were dissolved in Savillex screw-top PFA beakers using sequential addition of  
212 concentrated HF-HNO<sub>3</sub> (3:1), HCl-HNO<sub>3</sub> (3:1), and HNO<sub>3</sub>. The dissolved sample solutions were  
213 refluxed with and redissolved in 0.5 mol/L HNO<sub>3</sub>.

## 214 2.2 Potassium purification and isotope measurement

215 Potassium was isolated from other elements by cation-exchange chromatography described in  
216 Xu et al. (2019). Two mL of Bio-Rad AG 50W-X8 cation exchange resin (200-400 mesh) was  
217 filled into pre-cleaned Bio-Rad Poly-Prep columns. The resin was cleaned by three passes with 6  
218 mol/L HCl, one pass with 6 mol/L HNO<sub>3</sub>, and one pass with 1 mol/L HNO<sub>3</sub>. Each acid pass was  
219 rinsed with 10 mL of Milli-Q deionized water. The resin was then conditioned with 10 mL of 0.5  
220 mol/L HNO<sub>3</sub>. Dissolved sample solutions were loaded onto the resin in 1 mL of 0.5 mol/L HNO<sub>3</sub>.  
221 A volume of 13 mL of 0.5 mol/L HNO<sub>3</sub> was passed through the column, and the K fraction was  
222 collected in the subsequent 22 mL of the same acid. The sample solutions were passed through the  
223 column four times.

224 Potassium isotopic analyses followed the protocol described by Moynier et al. (2021). Purified  
225 K fractions were diluted in 0.5 mol/L HNO<sub>3</sub> to have K concentrations between 60 ppb and 70 ppb  
226 K. They were introduced into the mass spectrometer using an Apex Omega desolvation nebulizer  
227 system fitted with a 100 μL/min nebulizer. The ion beam was first decelerated to enter a hexapole  
228 collision cell to remove interfering species (e.g., <sup>40</sup>ArH<sup>+</sup> on <sup>41</sup>K<sup>+</sup>), and the <sup>41</sup>K<sup>+</sup> and <sup>39</sup>K<sup>+</sup> ion beams  
229 were accelerated and directed through the magnet to the Faraday collector. Each analysis consisted  
230 of a 90-second transfer time, a 60-second zero measurement in a blank solution, and 50 cycles of  
231 sample measurement with 5-second integration. A 150-second wash was performed between  
232 analyses. Each sample solution was paired with a standard solution diluted to the same K  
233 concentration (to within 2%). Standard and sample solutions were analyzed alternatively during a  
234 sequence to correct for instrumental mass bias. Potassium isotopic data are reported as the average  
235 of repeated analyses (4 to 8 times) relative to NIST SRM 3141a in delta notation:

$$236 \quad \delta^{41}\text{K} (\text{‰}) = \left\{ \frac{\left( \frac{{}^{41}\text{K}}{{}^{39}\text{K}} \right)_{\text{sample}}}{\left( \frac{{}^{41}\text{K}}{{}^{39}\text{K}} \right)_{\text{NIST SRM 3141a}}} - 1 \right\} \times 1000$$

237 Analytical uncertainties are reported as 2SD (standard deviation) and 95% c.i. (confidence  
238 interval) in Table 1 and Table S1. In the following sections, analytical uncertainty used for  
239 individual sample is 95% c.i. and that used for group average is 2SD unless stated otherwise.

240

## 241 **3 Results and discussions**

### 242 **3.1 Analytical accuracy**

243 We first evaluate the accuracy of our analyses by comparing the  $\delta^{41}\text{K}$  values of representative  
244 terrestrial standards and chondrites from analyses in this study to previous results. The  $\delta^{41}\text{K}$  values  
245 of basalt BIR ( $-0.418 \pm 0.031\text{‰}$ ) and BCR-2 ( $-0.426 \pm 0.030\text{‰}$ ), andesite AGV-2 ( $-0.455 \pm$   
246  $0.030\text{‰}$ ), and Pacific seawater ( $0.126 \pm 0.028\text{‰}$ ) analyzed during the course of this study agree  
247 well with published results (Chen et al., 2019; Hille et al., 2019; Hu et al., 2018; Moynier et al.,  
248 2021; Xu et al., 2019). In addition, Orgueil ( $-0.081 \pm 0.066\text{‰}$ ), Murchison ( $-0.250 \pm 0.043\text{‰}$ ),  
249 Allende ( $-0.169 \pm 0.030\text{‰}$ ), Cold Bokkeveld ( $-0.267 \pm 0.035\text{‰}$ ), and Lancé ( $-0.382 \pm 0.040\text{‰}$ )  
250 processed and analyzed in this study yielded consistent values with our previous analyses (Hu et  
251 al., 2022; Hu et al., 2023). This consistency confirms the accuracy of our analyses.

252 We then evaluate whether the multi-stage chemical separation procedures performed at Tokyo  
253 Tech affected the isotopic compositions of K in the samples. For Tagish Lake, the K extracted  
254 from the K-Mg-Ni fraction has a  $\delta^{41}\text{K}$  value of  $-0.180 \pm 0.049\text{‰}$ , which is indistinguishable from  
255 the values obtained from two new dissolutions of separate pieces of this meteorite from Tokyo  
256 Tech ( $-0.215 \pm 0.043\text{‰}$ ) and IPGP ( $-0.215 \pm 0.032\text{‰}$ ). Likewise, the K purified from the K-Mg-  
257 Ni fraction of Tarda ( $-0.223 \pm 0.037\text{‰}$ ) is isotopically identical to that purified from a separate  
258 piece of this meteorite at IPGP ( $-0.205 \pm 0.024\text{‰}$ ). This similarity in  $\delta^{41}\text{K}$  values suggests that the  
259 preliminary chemical processing performed at Tokyo Tech affects K negligibly. In support of this  
260 inference, the anion resin used to separate Zn from other constituent elements in the samples should  
261 not retain any  $\text{K}^+$ , which would be eluted from the resin. Therefore, it is reasonable to assume that  
262 the  $\delta^{41}\text{K}$  values of K extracted from the K-Mg-Ni fraction of the three Ryugu samples are  
263 representative of these samples.

264

### 265 **3.2 K isotopic compositions of CI chondrites and the bulk Solar System**

266 The three Ryugu samples have K abundances that are comparable to those of the CI chondrites  
267 (Fig. 1A). In addition, they display consistent  $\delta^{41}\text{K}$  values (Fig. 1B), with no significant differences  
268 between the samples collected from the touchdown site 1 (Chamber A sample A0106 =  $-0.172 \pm$

269 0.039‰) and the touchdown site 2 (Chamber C samples C0107 =  $-0.204 \pm 0.048\text{‰}$  and C0108 =  
270  $-0.207 \pm 0.055\text{‰}$ ). Furthermore, the two samples from Chamber C have essentially identical  $\delta^{41}\text{K}$   
271 values, indicating that the extraction of soluble organic matter from samples C0107 and A0106  
272 prior to K separation did not affect their K isotopic compositions. The three Ryugu samples yield  
273 an average  $\delta^{41}\text{K}$  value of  $-0.194 \pm 0.038\text{‰}$  (2SD), which falls within the range of CI chondrites  
274 (Fig. 1B). This result is consistent with previous observations of CI-like isotopic compositions of  
275 Ryugu for the moderately volatile elements Zn and Cu (Paquet et al., 2022) and the more refractory  
276 elements Fe, Cr, Ti, and Ca (Hopp et al., 2022; Moynier et al., 2022; Yokoyama et al., 2022).  
277 Potassium isotopes thus further strengthens the compositional links between Ryugu and CI  
278 chondrites.

279 The new data from Ryugu samples provide critical constraints on the K isotopic composition  
280 of the bulk Solar System, which can otherwise only be inferred from CI chondrites. Previous  
281 analyses of CI chondrites show highly variable  $\delta^{41}\text{K}$  values from  $-0.534\text{‰}$  to  $-0.039\text{‰}$ , covering  
282 almost the entire variation measured in carbonaceous chondrites (Hu et al., 2022; Hu et al., 2023;  
283 Koefoed et al., 2023; Koefoed et al., 2022; Ku and Jacobsen, 2020; Nie et al., 2021; Wang and  
284 Jacobsen, 2016). Ku and Jacobsen (2020) found that the lowest  $\delta^{41}\text{K}$  values were measured for a  
285 piece of Orgueil contaminated with 8% of continental crust material, resulting in its substantially  
286 higher K abundance and lower  $\delta^{41}\text{K}$  value than other Orgueil samples (Fig. 1). In comparison, the  
287 majority of K isotopic analyses on Orgueil show a limited variation from  $-0.220\text{‰}$  to  $-0.039\text{‰}$ ,  
288 except for two specimens with relatively higher K concentrations ( $\sim 700$  ppm) that might also be  
289 affected by crustal contamination (Fig. 1B). Excluding these two lower  $\delta^{41}\text{K}$  values, the analyses  
290 on nine separate samples of Orgueil give an average  $\delta^{41}\text{K}$  value of  $-0.159 \pm 0.118\text{‰}$  (2SD),  
291 suggesting a largely homogeneous K isotopic composition in Orgueil.

292 Unlike Orgueil, however, there is a large discrepancy in the  $\delta^{41}\text{K}$  values reported for two  
293 separate analyses of the CI-type specimen Ivuna. The lower value of  $-0.460 \pm 0.046\text{‰}$  does not  
294 appear to reflect terrestrial contamination because this Ivuna sample has a normal K abundance  
295 (458 ppm, Nie et al., 2021) as the uncontaminated Orgueil samples and the other Ivuna sample,  
296 which has a  $\delta^{41}\text{K}$  value ( $-0.180 \pm 0.060\text{‰}$ ) similar to the Orgueil (Fig. 1B). The lower Ivuna value  
297 is thus likely an unrepresentative sampling of the bulk Ivuna composition. This inference is  
298 supported by the heterogenous distribution of soluble elements in CI chondrites, in particular for  
299 Ivuna (Barrat et al., 2012; Brearley, 2006; Morlok et al., 2006; Palme and Zipfel, 2022) (Fig. 1A).

300 Excluding the anomalous Ivuna value, representative analyses of Ryugu and CI chondrites define  
301 an average  $\delta^{41}\text{K}$  value of  $-0.178 \pm 0.075\%$  (95% c.i.), which is currently the best estimate of the  
302 K isotopic composition of the bulk Solar System.

303

### 304 **3.3 Origin of K isotopic variations in carbonaceous chondrites**

305 A well-established average  $\delta^{41}\text{K}$  value of CI chondrites is an important reference for  
306 understanding the origin of K isotopic variations among different carbonaceous chondritic groups.  
307 This is because CI chondrites are generally used to approximate the isotopic composition of the  
308 matrix component in carbonaceous chondrites (e.g., Alexander, 2005; Braukmüller et al., 2018).  
309 Due to the lack of a robust  $\delta^{41}\text{K}$  value for CI chondrites in previous studies, a wide range of  $\delta^{41}\text{K}$   
310 values ( $-0.28$  to  $2.1\%$ ) was invoked for chondrules to explain K isotopic variations in  
311 carbonaceous chondrites (Bloom et al., 2020). The average  $\delta^{41}\text{K}$  values established for CI  
312 chondrites and Ryugu samples in this study agree with each other within uncertainty (Fig. 2). Their  
313  $\delta^{41}\text{K}$  values also overlap within uncertainty with those of the two ungrouped C2 chondrites (Tagish  
314 Lake and Tarda), which contain the second-highest matrix volume among carbonaceous chondrites  
315 (Fig. 2). These observations indicate that the CI-like matrix in carbonaceous chondrites is largely  
316 homogeneous in  $\delta^{41}\text{K}$ .

317 Compared with CI chondrites and Ryugu samples, carbonaceous chondrites from the CM  
318 (Murchison), CO (Lance), and CV (Allende) groups are variably depleted in the heavier K isotope,  
319 and their  $\delta^{41}\text{K}$  values correlate positively with the  $\delta^{66}\text{Zn}$  and  $\delta^{65}\text{Cu}$  values (Fig. 2). Positive  
320 correlations are also evident between  $\delta^{41}\text{K}$  with isotopes of other MVEs, including Rb, Sn, and Te,  
321 in a larger dataset of carbonaceous chondrites (Hu et al., 2023; Koefoed et al., 2023; Nie et al.,  
322 2021). These systematic correlations reflect the early formation of two nebular reservoirs, with a  
323 volatile-depleted refractory component such as chondrules or Ca-Al-rich inclusions (CAIs)  
324 carrying the light isotopic signatures, and a CI-like reservoir with the heaviest isotopic  
325 compositions, as initially proposed by Luck et al. (2005; 2003). This interpretation is consistent  
326 with a broad negative correlation between  $\delta^{41}\text{K}$  and  $1/[\text{K}]$  reported by Nie et al. (2021) for seven  
327 carbonaceous chondrites, from which they extrapolated a  $\delta^{41}\text{K}$  value of  $-0.33 \pm 0.12\%$  for the  
328 chondrule component and of  $0.04 \pm 0.08\%$  for the matrix component. When all available data are  
329 considered, there is a coinciding increase in  $\delta^{41}\text{K}$  with water content (as a proxy for matrix content)

330 and a decrease in  $\delta^{41}\text{K}$  with chondrule content in chondrites, further substantiating the role of  
331 chondrules as the carriers of K depletion and low- $\delta^{41}\text{K}$  signature in chondrites (Hu et al., 2023).  
332 Therefore, the inter-group K isotopic variations in carbonaceous chondrites primarily reflect  
333 variable mixing between the two main K hosts, i.e., chondrules and the matrix, accreted by the  
334 parent bodies of carbonaceous chondrites.

335

### 336 **3.4 K isotopic evidence for widespread aqueous alteration on chondrite parent bodies**

337 Although chondrule-matrix mixing could explain the inter-group  $\delta^{41}\text{K}$  variation among  
338 carbonaceous chondrites, the significant variability within individual chondrites remains  
339 perplexing. In addition to the anomalously low  $\delta^{41}\text{K}$  value reported for Ivuna, substantial  
340 variability has also been documented for Allende and Murchison. Our in-house Allende sample  
341 has a higher  $\delta^{41}\text{K}$  value ( $-0.169 \pm 0.030\text{‰}$ ) than the sample provided by the Smithsonian Museum  
342 ( $-0.292 \pm 0.044\text{‰}$ ), while they both fall within the previously reported range of  $-0.620\text{‰}$  to  
343  $-0.080\text{‰}$  for Allende (Bloom et al., 2020; Jiang et al., 2021a; Koefoed et al., 2023; Ku and  
344 Jacobsen, 2020; Nie et al., 2021). Furthermore, the Allende sample provided by the Smithsonian  
345 Museum is an aliquot from a large batch of homogenized powder, and its  $\delta^{41}\text{K}$  value is in the  
346 middle of the reported range. Our Murchison sample also has a  $\delta^{41}\text{K}$  value ( $-0.250 \pm 0.043\text{‰}$ ) that  
347 is in the middle of the previously reported range for Murchison ( $-0.410\text{‰}$  to  $-0.101\text{‰}$ , Jiang et  
348 al., 2021b; Koefoed et al., 2023; Ku and Jacobsen, 2020; Nie et al., 2021).

349 To identify the cause of intra-chondrite isotopic variability, we compare the two sets of  $\delta^{41}\text{K}$   
350 vs.  $\delta^{87}\text{Rb}$  data obtained from IPGP and those reported in Nie et al. (2021), respectively, for four  
351 carbonaceous chondrites. While the two datasets differ by varying extents for individual  
352 chondrites, the  $\delta^{41}\text{K}$  and  $\delta^{87}\text{Rb}$  values correlate in both datasets (Fig. 3A). For example, the  
353 Murchison specimen analyzed at IPGP has both lower  $\delta^{41}\text{K}$  and  $\delta^{87}\text{Rb}$  values than the specimen  
354 reported by Nie et al. (2021). The correlation between  $\delta^{41}\text{K}$  and  $\delta^{87}\text{Rb}$  values suggests that the  
355 variability reflects isotopic heterogeneity at the analyzed sample scale. This isotopic heterogeneity  
356 could reflect different proportions of chondrules present in the two different specimens of a given  
357 chondrite. In this case, the specimen containing more chondrules should have a lower K abundance  
358 and a lower  $\delta^{41}\text{K}$  value because chondrules are inferred to be depleted in K and its lighter isotope  
359 compared with the matrix, as indicated by the mixing curve in Fig. 3B. However, the specimen

360 with the lower K abundance is often found to have a higher  $\delta^{41}\text{K}$  value than that with the higher K  
361 abundance of the same chondrite (Fig. 3B), which is opposite to the expectation of mixing between  
362 varying proportions of chondrules with the matrix. Therefore, the observed sample heterogeneity  
363 cannot be due to the chondrule nugget effect alone but, to a greater extent, reflects the redistribution  
364 of K and its isotopes during aqueous alteration in chondrite parent bodies, which significantly  
365 altered the original K abundances and isotopic compositions in chondrules and matrix.

366 The effects of asteroidal aqueous alteration on the redistribution of alkalis in carbonaceous  
367 chondrites have been well documented, including the formation of diverse K-bearing phyllosilicate  
368 phases at  $< 100^\circ\text{C}$  and/or anhydrous phases (e.g., nepheline and sodalite) due to Fe-alkali-halogen  
369 metasomatism at  $\sim 200^\circ\text{-}300^\circ\text{C}$  (e.g., Brearley, 2014; Ikeda and Kimura, 1996; Kimura and Ikeda,  
370 1998; Krot et al., 1998; Krot et al., 1995). Ordinary chondrites also show signs, albeit more subtle,  
371 of interaction with aqueous fluids at varying temperatures, ranging from low-temperature  
372 alteration ( $< 200^\circ\text{C}$ , in the least-equilibrated petrologic type 3) to fluid-assisted metamorphism  
373 ( $200\text{-}400^\circ\text{C}$ , in petrologic types of 4-6). Before or during the earliest stage of thermal  
374 metamorphism, aqueous fluids were suggested to have flowed through the fine-grained matrix,  
375 dissolving the mesostasis near the edge of chondrules and migrating alkalis into chondrule cores  
376 (e.g., Grossman et al., 2000; Grossman and Brearley, 2005). The presence of fluids is evidenced  
377 by the brine-bearing salt crystals found in the Monahans and Zag ordinary chondrites, which are  
378 argued to represent fluid samples from the early Solar System (Rubin et al., 2002; Zolensky et al.,  
379 1999). More recently, fluid activity on S-type asteroids is further supported by nanometer-sized  
380 halite crystals detected in particles returned from the asteroid Itokawa by JAXA's Hayabusa  
381 mission (Che and Zega, 2023). These observations collectively suggest the widespread action of  
382 fluids on primitive asteroids in the early Solar System.

383 Fluid-rock interactions have also been invoked to explain K isotopic variations in chondritic  
384 components of the Allende and Hamlet (LL4) chondrites (Jiang et al., 2021a; Koefoed et al., 2020).  
385 While inter-group variations in  $\delta^{41}\text{K}$  are attributable to mixing between a CI-like matrix and K-  
386 poor, isotopically light chondrules, direct measurements on Allende and Hamlet show highly  
387 variable  $\delta^{41}\text{K}$  in chondrules with values both higher and lower than those of the matrices (Fig. 3C  
388 and D). Furthermore, CAIs formed well above the condensation temperature of K contain  
389 anomalously high K concentrations and  $\delta^{41}\text{K}$  values. These observations are inconsistent with the  
390 low  $\delta^{66}\text{Zn}$  and  $\delta^{71}\text{Ga}$  values measured in CAIs interpreted as reflecting incomplete condensation

391 (Kato et al., 2017; Luck et al., 2005). Instead of pristine nebular signatures, Jiang et al. (2021a)  
392 considered the high  $\delta^{41}\text{K}$  values of CAIs as a secondary feature inherited from aqueous fluids  
393 assuming that most K in the CAIs was secondary in origin (Fig. 3C). Furthermore, they proposed  
394 that as the fluids interact with the porous matrix, the heavier K isotope was preferentially leached  
395 from the matrix and entered chondrules or CAIs, overprinting the original K abundances and  
396 isotopic signatures of the chondritic components.

397 The preference for the heavier K isotope by aqueous fluids is supported by the direction of K  
398 isotope fractionation during chemical weathering on Earth. Global rivers ( $-0.59\text{‰}$  to  $0.12\text{‰}$ ) and  
399 oceans ( $0.12 \pm 0.07\text{‰}$ , 2SD) have heavier K isotopic compositions (Hille et al., 2019; Li et al.,  
400 2019; Wang et al., 2020; Wang et al., 2021) than fresh basaltic rocks averaging at  $-0.42 \pm 0.08\text{‰}$   
401 (2SD) (Hu et al., 2021; Tuller-Ross et al., 2019a; Tuller-Ross et al., 2019b). In addition, studies of  
402 weathering profiles and riverine sediments indicate that aqueous fluids preferentially leach the  
403 heavy K isotope from the bedrock with apparent isotope fractionation factors of  $0.08\text{‰}$  to  $0.55\text{‰}$ ,  
404 leaving behind isotopically light weathered residues (down to  $-0.94\text{‰}$ , Chen et al., 2020; Li et al.,  
405 2019; Teng et al., 2020). Consistent with field analyses, theoretical calculations based on K-O  
406 bond strengths also suggest an enrichment of the heavier K isotope in aqueous solutions relative  
407 to typical silicate minerals and a fractionation factor of  $0.24\text{‰}$  between aqueous fluids and illite  
408 (Zeng et al., 2019).

409 At the onset of aqueous alteration, the K abundance and  $\delta^{41}\text{K}$  value of matrix would have  
410 decreased, while the chondrules or CAIs would have increased K abundances and  $\delta^{41}\text{K}$  values.  
411 With increasing degrees of alteration, chondrules, CAIs, and matrix would tend to approach  
412 equilibrium. The significant  $\delta^{41}\text{K}$  variability in Allende and Murchison (Fig. 2) and the fact that  
413 the specimen with a lower K abundance typically has a higher  $\delta^{41}\text{K}$  value (Fig. 3B) suggest that  
414 these chondrites record early stages of aqueous alteration. A broad negative correlation between  
415  $\delta^{41}\text{K}$  values and K abundances is also observed in major groups of carbonaceous chondrites (Fig.  
416 S1), suggesting that aqueous alteration and associated redistribution of K isotopes occurred  
417 pervasively in the parent bodies of carbonaceous chondrites. Therefore, K isotopic variations in  
418 carbonaceous chondrites record volatility-driven isotope fractionations during chondrule  
419 formation, variable chondrule-matrix mixing at the accretion of chondrite parent bodies, and post-  
420 accretionary redistribution of K in chondrite parent bodies assisted by aqueous fluids.

421

## 422 **4 Conclusions**

423 Previous estimates of the K isotopic composition of the bulk Solar System were based solely  
424 on CI chondrites, which yielded inconsistent results that made it challenging to interpret  $\delta^{41}\text{K}$   
425 variability in planetary materials. This study reports the K isotopic composition of the first samples  
426 returned from a carbonaceous asteroid (Ryugu) by JAXA's Hayabusa2 mission. The Ryugu  
427 samples are free of terrestrial contamination, thereby, represent a pristine analogue of CI  
428 chondrites. Three aliquots of Ryugu particles were analyzed, yielding similar  $\delta^{41}\text{K}$  values between  
429  $-0.207\text{‰}$  and  $-0.172\text{‰}$ . This range is consistent with the K isotopic compositions of most CI  
430 chondrites except for lower  $\delta^{41}\text{K}$  values found in contaminated Orgueil samples and an  
431 anomalously low value previously reported for Ivuna. The lack of K enrichment in this Ivuna  
432 sample suggests that its anomalously low  $\delta^{41}\text{K}$  value does not reflect terrestrial contamination but  
433 is more likely an unrepresentative sampling of its bulk composition due to compositional  
434 heterogeneity at the sampled size. Considerable K isotopic heterogeneity is also observed in other  
435 carbonaceous chondrites and within individual chondritic groups, whereby  $\delta^{41}\text{K}$  values are broadly  
436 negatively correlated with K abundances. These observations suggest the widespread  
437 redistribution of K and its isotopes during aqueous alteration in chondrite parent bodies.

438

## 439 **Acknowledgements**

440 We thank Julien Moureau and Tu-Han Luu for their assistance with mass spectrometer  
441 maintenance. This work was partly supported by the IPGP analytical platform PARI, Region Ile-  
442 de-France SESAME Grants no. 12015908, and DIM ACAV+, the ERC grant agreement No.  
443 101001282 (METAL) (F.M.), the UnivEarthS Labex program (numbers: ANR-10-LABX-0023  
444 and ANR-11-IDEX-0005-02) (F.M.), JSPS Kaken-hi grants (S.T., H.Y., T.Y.), and the CNES.

445

446 The authors declare no conflicts of interest.

447

448 All data referred to in this article can be found in the tables or cited references.

449

450 **Tables**

451 **Table 1.** Potassium abundance (ppm) and isotopic composition (‰) of Ryugu samples and  
 452 carbonaceous chondrites analyzed in this study.

Sample	Group	$\delta^{41}\text{K}$ (‰)	2SD (‰)	95%c.i. (‰)	N	[K] (ppm)
<b>Ryugu particles</b>						
A0106		-0.150	0.065	0.060	4	436
duplicate		-0.172	0.085	0.056	5	
repeat		-0.191	0.059	0.048	5	
Wtd average		-0.172	0.040	0.039		
C0107		-0.192	0.070	0.040	6	457
duplicate		-0.214	0.066	0.056	5	
Wtd average		-0.204	0.030	0.048		
C0108		-0.188	0.086	0.059	5	604
repeat		-0.220	0.072	0.069	4	
Wtd average		-0.207	0.045	0.055		
Ryugu average		-0.194	0.038			
<b>Carbonaceous chondrites</b>						
Orgueil	C11	-0.081	0.070	0.066	5	568
Tagish lake-1	C2-ung	-0.178	0.097	0.050	5	358
duplicate		-0.181	0.057	0.048	5	
replicate		-0.215	0.057	0.043	6	
Wtd average		-0.195	0.042	0.037		
Tagish lake-2		-0.201	0.042	0.023	8	360
repeat		-0.236	0.051	0.03	7	
Wtd average		-0.215	0.049	0.032		
Tagish lake average		-0.205	0.029			
Tarda-1	C2-ung	-0.217	0.067	0.054	6	416
duplicate		-0.230	0.076	0.037	4	
repeat		-0.224	0.056	0.045	5	
Wtd average		-0.223	0.013	0.037		
Tarda-2		-0.166	0.063	0.050	5	416
repeat		-0.222	0.054	0.047	5	
repeat		-0.218	0.058	0.039	4	
replicate		-0.204	0.056	0.038	7	
duplicate		-0.189	0.060	0.047	6	
repeat		-0.222	0.060	0.050	5	
Wtd average		-0.205	0.044	0.024		
Tarda average		-0.214	0.026			
Murchison	CM2	-0.250	0.049	0.043	7	411
Cold Bokkeveld	CM2	-0.267	0.064	0.035	7	476
Lancé	CO3.5	-0.382	0.087	0.040	7	429.9
Allende (A)-1	CV3	-0.293	0.056	0.052	5	296
repeat		-0.292	0.072	0.048	5	
Wtd average		-0.292	0.001	0.044		
Allende-2		-0.151	0.062	0.059	5	267
repeat		-0.181	0.062	0.055	4	
repeat		-0.168	0.052	0.045	6	
replicate		-0.178	0.065	0.031	4	
Wtd average		-0.169	0.027	0.030		

453 Note: 'repeat' indicates repeat instrumental analysis. 'duplicate' indicate repeat column chemistry and instrumental  
 454 analysis. 'replicate' indicates repeat sample dissolution, column chemistry, and instrumental analysis. The number '-1'  
 455 and '-2' attached to the same names indicate different pieces of a given chondrite.

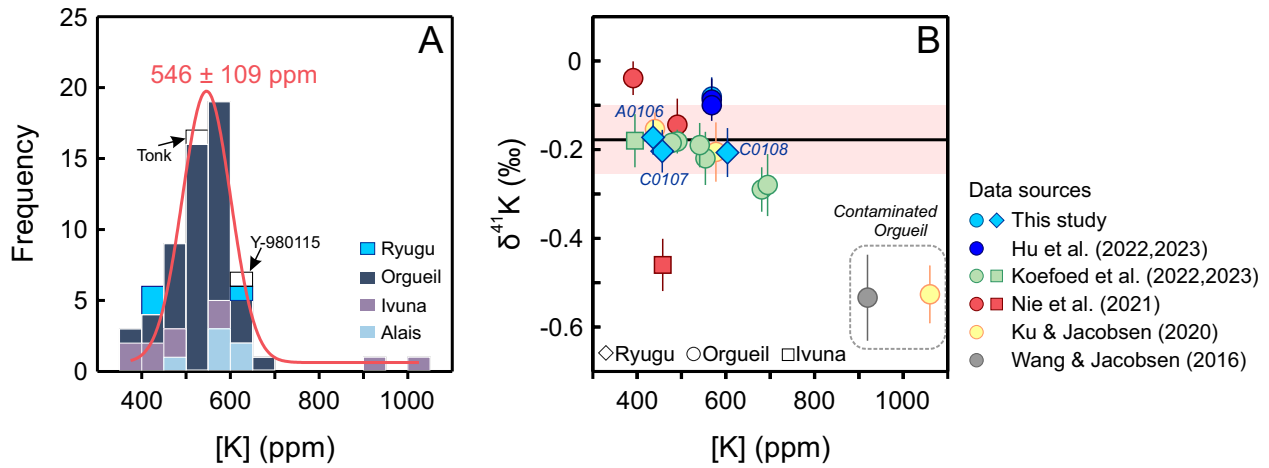
456 **Table S1.** Potassium isotopic compositions (‰) of terrestrial samples analyzed in this study.

Geostandard	Description	$\delta^{41}\text{K}$ (‰)	2SD (‰)	95%c.i. (‰)	N
BIR	Basalt	-0.448	0.059	0.036	7
replicate		-0.400	0.052	0.076	4
repeat		-0.414	0.050	0.062	4
Wtd average		-0.418	0.050	0.031	
BCR-2	Basalt	-0.404	0.051	0.019	8
repeat		-0.443	0.044	0.024	7
replicate		-0.425	0.066	0.034	5
Wtd average		-0.426	0.039	0.030	
AGV-2	Andesite	-0.455	0.042	0.030	7
Pacific seawater		0.152	0.060	0.054	4
repeat		0.128	0.078	0.050	6
repeat		0.113	0.039	0.037	7
repeat		0.133	0.084	0.056	5
Wtd average		0.126	0.032	0.028	

457

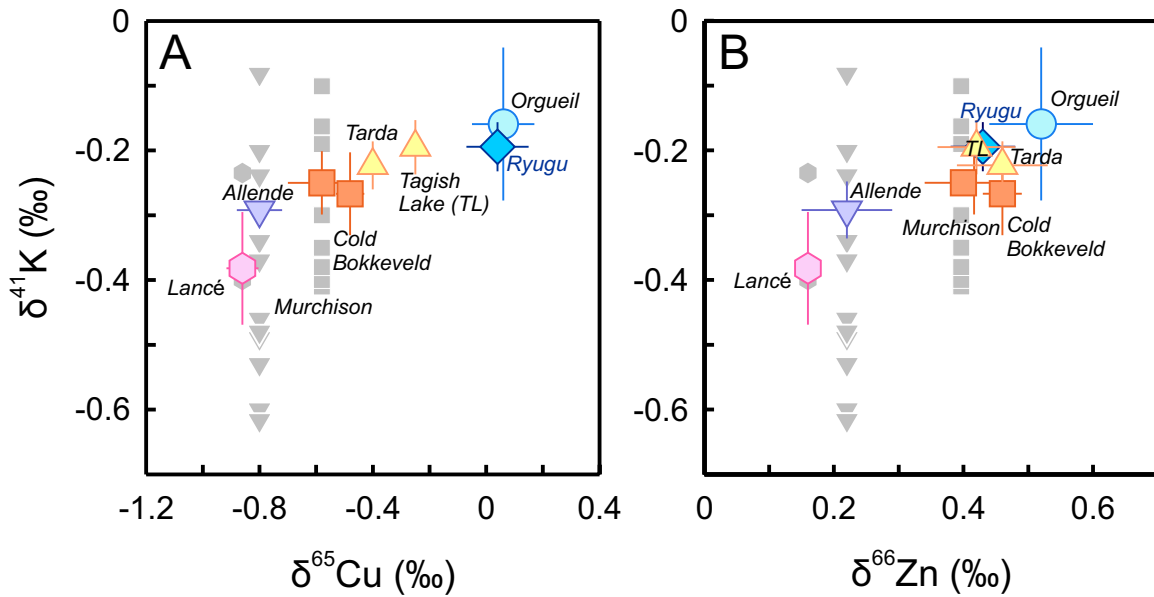
458 **Figures**

459



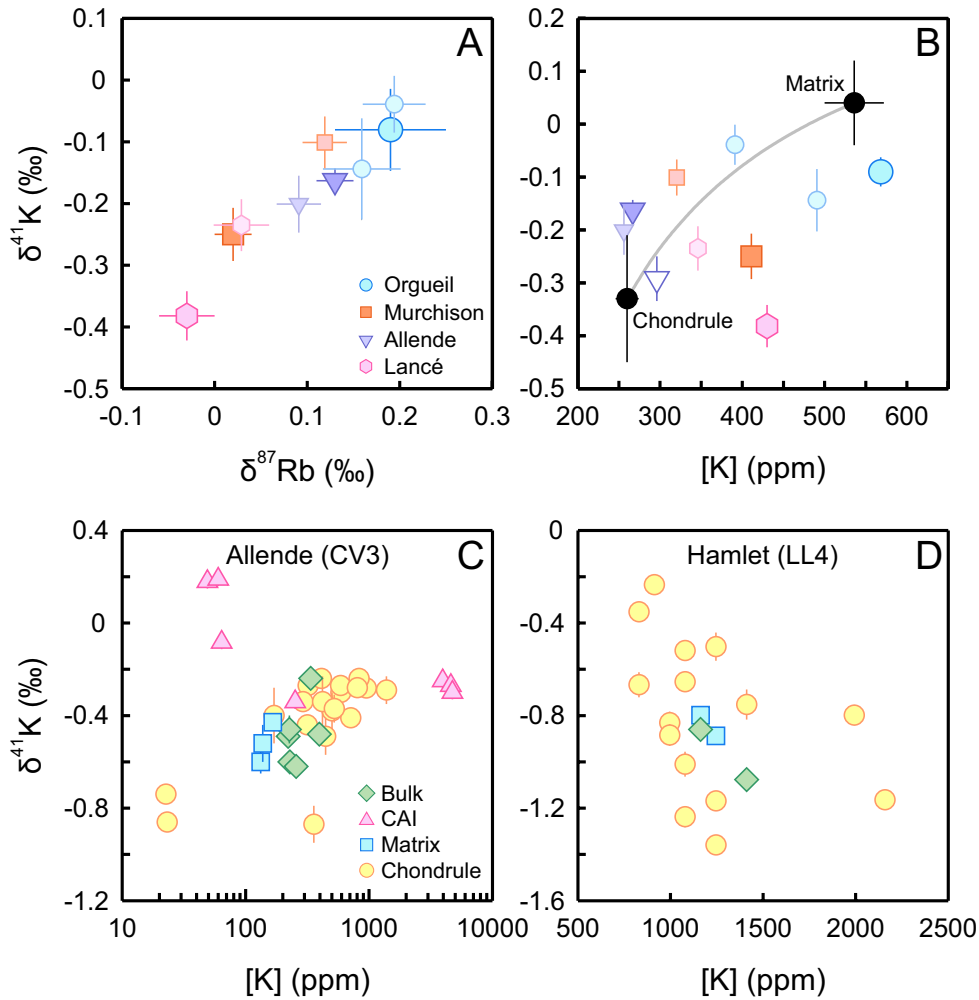
460

461 **Figure 1.** Potassium abundances ([K], ppm) and isotope compositions ( $\delta^{41}\text{K}$ , ‰) of CI chondrites  
 462 and Ryugu samples. (A) A histogram of K abundances in CI chondrites reported in the literature  
 463 (Ahrens et al., 1969; Anders and Grevesse, 1989; Barrat et al., 2012; Beer et al., 1984; Braukmüller  
 464 et al., 2018; Edwards and Urey, 1955; Jarosewich, 1990; Kallemeyn and Wasson, 1981; Kaushal  
 465 and Wetherill, 1970; Makishima and Nakamura, 2006; Mittlefehldt, 2002; Nakamura, 1974;  
 466 Nichiporuk and Moore, 1974; Palme and Zipfel, 2022; Von Michaelis et al., 1969; Wiik, 1956).  
 467 (B) The three aliquots of Ryugu particles have indistinguishable  $\delta^{41}\text{K}$  values and fall within the  
 468 range of CI chondrites except for an anomalously lower  $\delta^{41}\text{K}$  value previously reported for Ivuna.  
 469 The horizontal black line and pink field indicate the average  $\delta^{41}\text{K}$  value of Ryugu samples and CI  
 470 chondrites ( $-0.178 \pm 0.075$ ‰), representing the current best estimate of the bulk K isotopic  
 471 composition of the Solar System. Crustal contamination results in elevated K abundances and  
 472 crust-like, lower  $\delta^{41}\text{K}$  compared with pristine CI chondrite values (Ku and Jacobsen, 2020; Wang  
 473 and Jacobsen, 2016). The K abundance of Ryugu C0108 is from Yokoyama et al. (2022), while  
 474 those of A0106 and C0107 are new data reported in this study (Table 1).



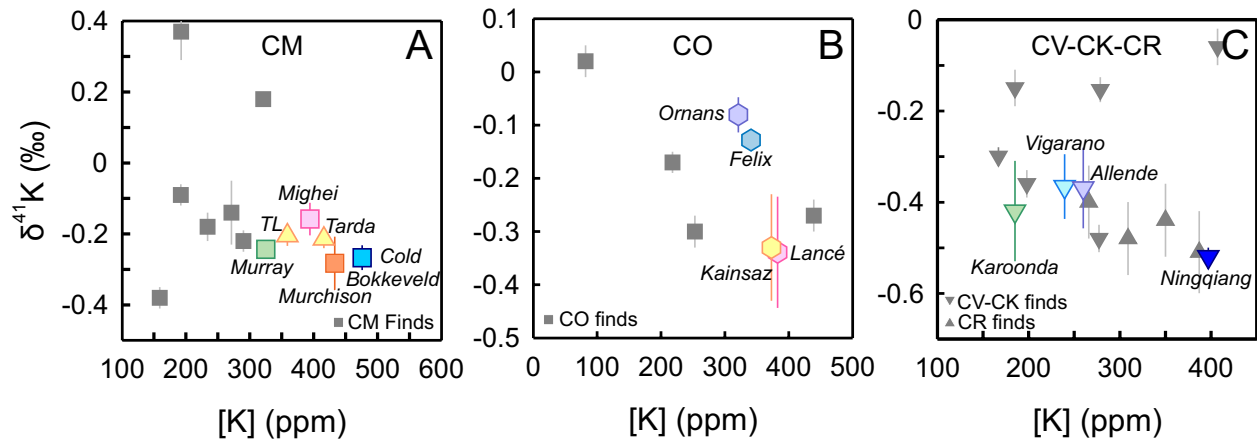
475

476 **Figure 2.** Positive correlations of  $\delta^{41}\text{K}$  values with (A)  $\delta^{65}\text{Cu}$  values and (B)  $\delta^{66}\text{Zn}$  values in Ryugu  
 477 samples and different groups of carbonaceous chondrites. These correlations suggest inter-group  
 478 variations in  $\delta^{41}\text{K}$  primarily reflect mixing of a CI-, or Ryugu-like matrix component with the  
 479 heaviest isotopic compositions and a volatile-depleted refractory component such as chondrules  
 480 carrying the light isotopic signatures. The colored symbols are data from this study and the grey  
 481 symbols are literature values. In (A),  $\delta^{41}\text{K}$  and  $\delta^{65}\text{Cu}$  values (Paquet et al., 2022) for Ryugu, Tarda,  
 482 Allende were measured from the same specimens.  $\delta^{65}\text{Cu}$  values for Orgueil and Murchison are  
 483 from Paquet et al. (2022), for Tagish Lake, Cold Bokkeveld, and Lancé are from Luck et al. (2003).  
 484 In (B),  $\delta^{41}\text{K}$  and  $\delta^{66}\text{Zn}$  values (Paquet et al., 2022; Pringle et al., 2017) for Ryugu, Tagish Lake,  
 485 Tarda, Murchison, Cold Bokkeveld, Lancé, and Allende were measured from the same specimens.  
 486  $\delta^{66}\text{Zn}$  value for Orgueil is from Paquet et al. (2022). Literature  $\delta^{41}\text{K}$  values are from Bloom et al.  
 487 (2020); Jiang et al. (2021a); Jiang et al. (2021b); Koefoed et al. (2023); Koefoed et al. (2022); Ku  
 488 and Jacobsen (2020); Nie et al. (2021). Although literature  $\delta^{41}\text{K}$  values were plotted with  $\delta^{65}\text{Cu}$   
 489 and  $\delta^{66}\text{Zn}$  values measured from different specimens of a given chondrite,  $\delta^{65}\text{Cu}$  and  $\delta^{66}\text{Zn}$  values  
 490 reported for different specimens of Orgueil, Murchison, and Allende generally agree well (Barrat  
 491 et al., 2012; Luck et al., 2005; Luck et al., 2003; Paquet et al., 2022; Pringle et al., 2017).



492

493 **Figure 3.** K isotopic evidence of aqueous alteration of chondrites on their parent bodies. (A)  
 494 Positively correlated  $\delta^{41}\text{K}$  and  $\delta^{87}\text{Rb}$  values indicate sample heterogeneity for a given chondrite.  
 495 The larger symbols are data from this study and the smaller symbols are from Nie et al. (2021).  
 496 (B) The broad positive correlation between  $\delta^{41}\text{K}$  values and K abundances across different  
 497 carbonaceous chondrite groups indicates mixing of the CI-like, isotopically heavy matrix with K-  
 498 depleted, isotopically light chondrules, as indicated by the mixing curve using endmember  
 499 compositions extrapolated in Nie et al. (2021). However, for a given chondrite (coded with the  
 500 same color), the specimen with the higher K abundance often has a lower  $\delta^{41}\text{K}$  value than that with  
 501 the lower K abundance. The large solid triangle down is an Allende specimen from IPGP, and the  
 502 open triangle down is an aliquot of pulverized Allende provided by the Smithsonian Museum. (C)  
 503 and (D)  $\delta^{41}\text{K}$  values measured in chondrules, calcium-aluminum-rich inclusions (CAIs), and  
 504 matrices in Allende and Hamlet chondrites show significant alteration of the original K abundances  
 505 and  $\delta^{41}\text{K}$  values of all chondritic components. Data source: Data presented in (A) and (B) are from  
 506 this study and the literature (Nie et al., 2021; Pringle and Moynier, 2017), whereas those presented  
 507 in (C) and (D) are from Jiang et al. (2021a); Ku et al. (2022), and Koefoed et al. (2020).



508

509 **Figure S1.**  $\delta^{41}\text{K}$  values of bulk carbonaceous chondrites from the CM, CO, CV-CK, and CR  
 510 groups as a function of K abundances. There is a broad negative correlation between  $\delta^{41}\text{K}$  values  
 511 and K abundances. These correlations are opposite to the positive correlations reflective of binary  
 512 mixing of varying proportions of K-depleted, isotopically light chondrules with the CI-like matrix  
 513 (also see the grey curve in Fig. 3B). Instead, the correlations suggest mixing between aqueously  
 514 altered chondrules (with elevated  $\delta^{41}\text{K}$  values) and matrix (with lowered  $\delta^{41}\text{K}$  values). The colored  
 515 symbols are witnessed falls and the grey symbols are chondrite finds. Data sources: this study and  
 516 literature values (Bloom et al., 2020; Hu et al., 2022; Hu et al., 2023; Jiang et al., 2021a; Jiang et  
 517 al., 2021b; Koefoed et al., 2023; Nie et al., 2021).

518 **References**

519 Ahrens, L. H., Von Michaelis, H., Fesq, H. W., 1969. The composition of the stony meteorites (IV) some  
520 analytical data on Orgueil, Nogoya, Ornans and Ngawi. *Earth and Planetary Science Letters*. 6,  
521 285-288.

522 Alexander, C. M. O. D., 2005. Re-examining the role of chondrules in producing the elemental  
523 fractionations in chondrites. *Meteoritics & Planetary Science*. 40, 943-965.

524 Anders, E., Grevesse, N., 1989. Abundances of the elements: Meteoritic and solar. *Geochimica et*  
525 *Cosmochimica Acta*. 53, 197-214.

526 Arakawa, M., et al., 2020. An artificial impact on the asteroid (162173) Ryugu formed a crater in the  
527 gravity-dominated regime. *Science*. 368, 67-71.

528 Barrat, J. A., Zanda, B., Moynier, F., Bollinger, C., Liorzou, C., Bayon, G., 2012. Geochemistry of CI  
529 chondrites: Major and trace elements, and Cu and Zn Isotopes. *Geochimica et Cosmochimica Acta*.  
530 83, 79-92.

531 Beer, H., Walter, G., Macklin, R. L., Patchett, P. J., 1984. Neutron capture cross sections and solar  
532 abundances of <sup>160,161</sup>Dy, <sup>170,171</sup>Yb, <sup>175,176</sup>Lu, and <sup>176,177</sup>Hf for the s-process analysis of the  
533 radionuclide <sup>176</sup>Lu. *Physical Review C*. 30, 464-478.

534 Bloom, H., et al., 2020. Potassium isotope compositions of carbonaceous and ordinary chondrites:  
535 Implications on the origin of volatile depletion in the early solar system. *Geochimica et*  
536 *Cosmochimica Acta*. 277, 111-131.

537 Braukmüller, N., Wombacher, F., Hezel, D. C., Escoube, R., Münker, C., 2018. The chemical composition  
538 of carbonaceous chondrites: Implications for volatile element depletion, complementarity and  
539 alteration. *Geochimica et Cosmochimica Acta*. 239, 17-48.

540 Brearley, A. J., 2006. The action of water. *Meteorites and the early solar system II*. 943, 587-624.

541 Brearley, A. J., 2014 1.9 - Nebular Versus Parent Body Processing. In: H. D. Holland, K. K. Turekian,  
542 (Eds.), *Treatise on Geochemistry (Second Edition)*. Elsevier, Oxford, pp. 309-334.

543 Che, S., Zega, T. J., 2023. Hydrothermal fluid activity on asteroid Itokawa. *Nature Astronomy*.

544 Chen, H., Liu, X.-M., Wang, K., 2020. Potassium isotope fractionation during chemical weathering of  
545 basalts. *Earth and Planetary Science Letters*. 539, 116192.

546 Chen, H., Tian, Z., Tuller-Ross, B., Korotev, Randy L., Wang, K., 2019. High-precision potassium isotopic  
547 analysis by MC-ICP-MS: an inter-laboratory comparison and refined K atomic weight. *Journal of*  
548 *Analytical Atomic Spectrometry*. 34, 160-171.

549 Clayton, R. N., 1993. Oxygen Isotopes in Meteorites. *Annual Review of Earth and Planetary Sciences*. 21,  
550 115-149.

551 Edwards, G., Urey, H. C., 1955. Determination of alkali metals in meteorites by a distillation process.  
552 *Geochimica et Cosmochimica Acta*. 7, 154-168.

553 Grossman, J. N., ALEXANDER, C. M. O. D., Wang, J., Brearley, A. J., 2000. Bleached chondrules:  
554 Evidence for widespread aqueous processes on the parent asteroids of ordinary chondrites.  
555 *Meteoritics & Planetary Science*. 35, 467-486.

556 Grossman, J. N., Brearley, A. J., 2005. The onset of metamorphism in ordinary and carbonaceous  
557 chondrites. *Meteoritics & Planetary Science*. 40, 87-122.

558 Hille, M., Hu, Y., Huang, T.-Y., Teng, F.-Z., 2019. Homogeneous and heavy potassium isotopic  
559 composition of global oceans. *Science Bulletin*. 64, 1740-1742.

560 Hopp, T., et al., 2022. Ryugu's nucleosynthetic heritage from the outskirts of the Solar System. *Science*  
561 *Advances*. 8, eadd8141.

562 Hu, Y., Chen, X.-Y., Xu, Y.-K., Teng, F.-Z., 2018. High-precision analysis of potassium isotopes by HR-  
563 MC-ICPMS. *Chemical Geology*. 493, 100-108.

564 Hu, Y., Moynier, F., Bizzarro, M., 2022. Potassium isotope heterogeneity in the early Solar System  
565 controlled by extensive evaporation and partial recondensation. *Nature Communications*. 13, 7669.

- 566 Hu, Y., Moynier, F., Yang, X., 2023. Volatile-depletion processing of the building blocks of Earth and  
567 Mars as recorded by potassium isotopes. *Earth and Planetary Science Letters*. 620, 118319.
- 568 Hu, Y., Teng, F.-Z., Helz, R. T., Chauvel, C., 2021. Potassium isotope fractionation during magmatic  
569 differentiation and the composition of the mantle. *Journal of Geophysical Research: Solid Earth*.  
570 126, e2020JB021543.
- 571 Ikeda, Y., Kimura, M., 1996. Anhydrous alteration of Allende chondrules in the solar nebula III: Alkali-  
572 zoned chondrules and heating experiments for anhydrous alteration. *Antarctic Meteorite Research*.  
573 9, 51.
- 574 Jarosewich, E., 1990. Chemical analyses of meteorites: A compilation of stony and iron meteorite analyses.  
575 *Meteoritics*. 25, 323-337.
- 576 Jiang, Y., et al., 2021a. Early solar system aqueous activity: K isotope evidence from Allende. *Meteoritics  
577 & Planetary Science*. 56, 61-76.
- 578 Jiang, Y., Koefoed, P., Wang, K., Xu, W.-B., 2021b. High precision potassium isotopic study of Chinese  
579 Antarctic chondrites. *Acta Geologica Sinica*. 95.
- 580 Kallemeyn, G. W., Wasson, J. T., 1981. The compositional classification of chondrites—I. The  
581 carbonaceous chondrite groups. *Geochimica et Cosmochimica Acta*. 45, 1217-1230.
- 582 Kato, C., Moynier, F., Foriel, J., Teng, F.-Z., Puchtel, I. S., 2017. The gallium isotopic composition of the  
583 bulk silicate Earth. *Chemical Geology*. 448, 164-172.
- 584 Kaushal, S. K., Wetherill, G. W., 1970. Rubidium 87-Strontium 87 age of carbonaceous chondrites. *Journal  
585 of Geophysical Research (1896-1977)*. 75, 463-468.
- 586 Kimura, M., Ikeda, Y., 1998. Hydrous and anhydrous alterations of chondrules in Kaba and Mokoia CV  
587 chondrites. *Meteoritics & Planetary Science*. 33, 1139-1146.
- 588 Kitazato, K., et al., 2019. The surface composition of asteroid 162173 Ryugu from Hayabusa2 near-infrared  
589 spectroscopy. *Science*. 364, 272-275.
- 590 Koefoed, P., et al., 2023. The potassium isotopic composition of CI chondrites and the origin of isotopic  
591 variations among primitive planetary bodies. *Geochimica et Cosmochimica Acta*.
- 592 Koefoed, P., Pravdivtseva, O., Chen, H., Gerritzen, C., Thiemens, M. M., Wang, K., 2020. Potassium  
593 isotope systematics of the LL4 chondrite Hamlet: Implications for chondrule formation and  
594 alteration. *Meteoritics & Planetary Science*. 55.
- 595 Koefoed, P., et al., 2022. The dynamic formation process of the CB chondrite Gujba. *Geochimica et  
596 Cosmochimica Acta*. 332, 33-56.
- 597 Krot, A. N., Petaev, M. I., Scott, E. R. D., Choi, B.-G., Zolensky, M. E., Keil, K., 1998. Progressive  
598 alteration in CV3 chondrites: More evidence for asteroidal alteration. *Meteoritics & Planetary  
599 Science*. 33, 1065-1085.
- 600 Krot, A. N., Scott, E. R. D., Zolensky, M. E., 1995. Mineralogical and chemical modification of components  
601 in CV3 chondrites: Nebular or asteroidal processing? *Meteoritics*. 30, 748-775.
- 602 Ku, Y., Jacobsen, S. B., 2020. Potassium isotope anomalies in meteorites inherited from the protosolar  
603 molecular cloud. *Science Advances*. 6, eabd0511.
- 604 Ku, Y., Petaev, M. I., Jacobsen, S. B., 2022. The Timing of Potential Last Nucleosynthetic Injections into  
605 the Protosolar Molecular Cloud Inferred from  $^{41}\text{Ca}$ - $^{26}\text{Al}$  Systematics  
606 of Bulk CAIs. *The Astrophysical Journal Letters*. 931, L13.
- 607 Li, S., et al., 2019. K isotopes as a tracer for continental weathering and geological K cycling. *Proceedings  
608 of the National Academy of Sciences*. 116, 8740-8745.
- 609 Luck, J.-M., Othman, D. B., Albarède, F., 2005. Zn and Cu isotopic variations in chondrites and iron  
610 meteorites: Early solar nebula reservoirs and parent-body processes. *Geochimica et Cosmochimica  
611 Acta*. 69, 5351-5363.
- 612 Luck, J. M., Othman, D. B., Barrat, J. A., Albarède, F., 2003. Coupled  $^{63}\text{Cu}$  and  $^{16}\text{O}$  excesses in chondrites.  
613 *Geochimica et Cosmochimica Acta*. 67, 143-151.

614 Makishima, A., Nakamura, E., 2006. Determination of major/minor and trace elements in silicate samples  
615 by ICP-QMS and ICP-SFMS applying isotope dilution-internal standardisation (ID-IS) and multi-  
616 stage internal standardisation. *Geostandards and Geoanalytical Research*. 30, 245-271.

617 McSween, H. Y., Ghosh, A., Grimm, R. E., Wilson, L., Young, E. D., 2002. Thermal evolution models of  
618 asteroids. *Asteroids III*. 559, 559-572.

619 Mittlefehldt, D. W., 2002. Geochemistry of the ungrouped carbonaceous chondrite Tagish Lake, the  
620 anomalous CM chondrite Bells, and comparison with CI and CM chondrites. *Meteoritics &  
621 Planetary Science*. 37, 703-712.

622 Morlok, A., Bischoff, A., Stephan, T., Floss, C., Zinner, E., Jessberger, E. K., 2006. Brecciation and  
623 chemical heterogeneities of CI chondrites. *Geochimica et Cosmochimica Acta*. 70, 5371-5394.

624 Morota, T., et al., 2020. Sample collection from asteroid (162173) Ryugu by Hayabusa2: Implications for  
625 surface evolution. *Science*. 368, 654-659.

626 Moynier, F., et al., 2022. The Solar System calcium isotopic composition inferred from Ryugu samples.  
627 *Geochemical Perspectives Letters*. 24, 1-6.

628 Moynier, F., et al., 2021. Potassium isotopic composition of various samples using a dual-path collision  
629 cell-capable multiple-collector inductively coupled plasma mass spectrometer, Nu instruments  
630 Sapphire. *Chemical Geology*. 571, 120144.

631 Nakamura, E., et al., 2022. On the origin and evolution of the asteroid Ryugu: A comprehensive  
632 geochemical perspective. *Proceedings of the Japan Academy, Series B*. 98, 227-282.

633 Nakamura, N., 1974. Determination of REE, Ba, Fe, Mg, Na and K in carbonaceous and ordinary  
634 chondrites. *Geochimica et Cosmochimica Acta*. 38, 757-775.

635 Naraoka, H., et al., 2023. Soluble organic molecules in samples of the carbonaceous asteroid (162173)  
636 Ryugu. *Science*. 379, eabn9033.

637 Nichiporuk, W., Moore, C. B., 1974. Lithium, sodium and potassium abundances in carbonaceous  
638 chondrites. *Geochimica et Cosmochimica Acta*. 38, 1691-1701.

639 Nie, N. X., et al., 2021. Imprint of chondrule formation on the K and Rb isotopic compositions of  
640 carbonaceous meteorites. *Science Advances*. 7, eabl3929.

641 Palme, H., Lodders, K., Jones, A., 2014 2.2 - Solar System abundances of the elements. In: H. D. Holland,  
642 K. K. Turekian, (Eds.), *Treatise on Geochemistry (Second Edition)*. Elsevier, Oxford, pp. 15-36.

643 Palme, H., Zipfel, J., 2022. The composition of CI chondrites and their contents of chlorine and bromine:  
644 Results from instrumental neutron activation analysis. *Meteoritics & Planetary Science*. 57, 317-  
645 333.

646 Paquet, M., et al., 2022. Contribution of Ryugu-like material to Earth's volatile inventory by Cu and Zn  
647 isotopic analysis. *Nature Astronomy*.

648 Pilorget, C., et al., 2022. First compositional analysis of Ryugu samples by the MicrOmega hyperspectral  
649 microscope. *Nature Astronomy*. 6, 221-225.

650 Pringle, E. A., Moynier, F., 2017. Rubidium isotopic composition of the Earth, meteorites, and the Moon:  
651 Evidence for the origin of volatile loss during planetary accretion. *Earth and Planetary Science  
652 Letters*. 473, 62-70.

653 Pringle, E. A., Moynier, F., Beck, P., Paniello, R., Hezel, D. C., 2017. The origin of volatile element  
654 depletion in early solar system material: Clues from Zn isotopes in chondrules. *Earth and Planetary  
655 Science Letters*. 468, 62-71.

656 Rubin, A. E., 2012. Collisional facilitation of aqueous alteration of CM and CV carbonaceous chondrites.  
657 *Geochimica et Cosmochimica Acta*. 90, 181-194.

658 Rubin, A. E., Zolensky, M. E., Bodnar, R. J., 2002. The halite-bearing Zag and Monahans (1998) meteorite  
659 breccias: Shock metamorphism, thermal metamorphism and aqueous alteration on the H-chondrite  
660 parent body. *Meteoritics & Planetary Science*. 37, 125-141.

661 Sugita, S., et al., 2019. The geomorphology, color, and thermal properties of Ryugu: Implications for  
662 parent-body processes. *Science*. 364, eaaw0422.

663 Tachibana, S., et al., 2022. Pebbles and sand on asteroid (162173) Ryugu: In situ observation and particles  
664 returned to Earth. *Science*. 375, 1011-1016.

665 Teng, F.-Z., Hu, Y., Ma, J.-L., Wei, G.-J., Rudnick, R. L., 2020. Potassium isotope fractionation during  
666 continental weathering and implications for global K isotopic balance. *Geochimica et*  
667 *Cosmochimica Acta*. 278, 261-271.

668 Tomeoka, K., Buseck, P. R., 1988. Matrix mineralogy of the Orgueil CI carbonaceous chondrite.  
669 *Geochimica et Cosmochimica Acta*. 52, 1627-1640.

670 Tuller-Ross, B., Marty, B., Chen, H., Kelley, K. A., Lee, H., Wang, K., 2019a. Potassium isotope  
671 systematics of oceanic basalts. *Geochimica et Cosmochimica Acta*. 259, 144-154.

672 Tuller-Ross, B., Savage, P. S., Chen, H., Wang, K., 2019b. Potassium isotope fractionation during  
673 magmatic differentiation of basalt to rhyolite. *Chemical Geology*. 525, 37-45.

674 Von Michaelis, H., Ahrens, L. H., Willis, J. P., 1969. The composition of stony meteorites. II. The analytical  
675 data and an assessment of their quality. *Earth and Planetary Science Letters*. 5, 387-394.

676 Wang, K., Close, H. G., Tuller-Ross, B., Chen, H., 2020. Global Average Potassium Isotope Composition  
677 of Modern Seawater. *ACS Earth and Space Chemistry*. 4, 1010-1017.

678 Wang, K., Jacobsen, S. B., 2016. Potassium isotopic evidence for a high-energy giant impact origin of the  
679 Moon. *Nature*. 538, 487-490.

680 Wang, K., Peucker-Ehrenbrink, B., Chen, H., Lee, H., Hasenmueller, E. A., 2021. Dissolved potassium  
681 isotopic composition of major world rivers. *Geochimica et Cosmochimica Acta*. 294, 145-159.

682 Wiik, H. B., 1956. The chemical composition of some stony meteorites. *Geochimica et Cosmochimica*  
683 *Acta*. 9, 279-289.

684 Xu, Y.-K., et al., 2019. Potassium isotopic compositions of international geological reference materials.  
685 *Chemical Geology*. 513, 101-107.

686 Yada, T., et al., 2022. Preliminary analysis of the Hayabusa2 samples returned from C-type asteroid Ryugu.  
687 *Nature Astronomy*. 6, 214-220.

688 Yokoyama, T., et al., 2022. Samples returned from the asteroid Ryugu are similar to Ivuna-type  
689 carbonaceous meteorites. *Science*. 0, eabn7850.

690 Zeng, H., et al., 2019. Ab Initio Calculation of Equilibrium Isotopic Fractionations of Potassium and  
691 Rubidium in Minerals and Water. *ACS Earth and Space Chemistry*. 3, 2601-2612.

692 Zolensky, M., McSween, H. Y., 1988 Aqueous alteration. In: J. F. Kerridge, M. S. Matthews, (Eds.),  
693 *Meteorites and the Early Solar System*, pp. 114-143.

694 Zolensky, M. E., et al., 1999. Asteroidal water within fluid inclusion-bearing halite in an H5 chondrite,  
695 Monahans (1998). *Science*. 285, 1377-1379.

696